Rock Mechanics and Rock Engineering (2023) 56:5241–5252
https://doi.org/10.1007/s00603-023-03334-y

ORIGINAL PAPER

Effect of Pore Pressure on Strain Rate-Dependency of Coal

Linan Su[1] · Mohammed Abdul Qadeer Siddiqui[1] · Hamid Roshan[1]

Received: 18 October 2022 / Accepted: 6 April 2023 / Published online: 15 April 2023

Abstract

Viscoelastic strain rate-dependent behaviour of coal is critical in several subsurface engineering applications especially coal seams gas production. Such rate dependency is controlled by the interaction between coal bulk and gas sorption (a sorbing gas) or gas pressure (a non-sorbing gas). Despite the research conducted to date, the gas pressure effect (non-sorbing) on the viscous behaviour of sediments in particular coal remains unexplored. We, therefore, investigate the strain rate-dependent mechanical behaviour of coal under isotropic loading to specifically explore the effect of gas pressure (Helium) on its rate dependency eliminating the sorption effect. We perform a set of triaxial experiments on coal specimens at dry and pressurised gas (Helium) conditions under different strain rates under isotropic loading. The experimental results show that all coal specimens have viscoelastic strain rate dependency at a dry condition where viscous effect increases with strain rate. As a result, the bulk modulus of the specimens increases with the increase in strain rates. This strain rate dependency response, however, reduces with an increase in pore pressure and vanishes at a certain pore pressure under the same effective stress to that of dry specimens. We further employ X-ray micro-Computed Tomography (XRCT) to 3D scan a coal specimen saturated with Krypton gas undergoing different loading rates to shed light on the micro-mechanisms of gas pressure effect on specimens' rate dependency. The XRCT results show that gas can be trapped in small-scale fractures and pores during the loading process leading to a localised undrained response that can stiffen the specimen and reduce its ability to show viscous rate dependency. The obtained results are significant in optimizing coal seam gas production and coal seam gas drainage applications.

Highlights

- A series of triaxial tests have been conducted on coal specimens to investigate the strain rate dependency.
- The experimental results from triaxial tests show clear strain rate dependency of coal specimens under dry conditions.
- The strain rate dependency decreases significantly with introducing Helium pore pressure and vanishes at certain pore pressure.
- The XRCT results show that the gas can be trapped inside the microfractures and pores under drained isotropic loading, causing a decrease in rate dependency.

Keywords Strain rate dependency · Undrained conditions · Poro-viscoelasticity · Triaxial compression · Fractured rocks

List of symbols

P_c Isotropic (hydrostatic) stress
p Pore pressure
ε_v Volumetric strain
K Bulk modulus
K_s Solid bulk modulus
α Biot coefficient
σ' Effective stress
σ_t Total stress

✉ Hamid Roshan
h.roshan@unsw.edu.au

[1] School of Minerals and Energy Resources Engineering, UNSW Australia, Sydney, NSW 2052, Australia

1 Introduction

Coal seams are a great source of natural gas supply to fulfill the current energy demands to a large extent. The optimisation of gas production from coal seams, however, offers significant challenges due to the complex structure of coal and coupled physical processes involved in gas production (Perera and Sampath 2020; Van Eeckhout 1976). Gas production from coal seam is a strong function of coal geomechanical behaviour thus accurate prediction of coal effective stress is important. The effective stress behaviour of coal is often described through dual continuum poroelasticity (Aghighi et al. 2021, 2022; Espinoza et al. 2016; Lv et al. 2021) because of its distinct fracture and matrix pore network. Previous experimental studies have, however, shown apparent viscoelastic deformation of coal under different loading strain rates (Cao et al. 2019; Song et al. 2021; Zhao et al. 2016); the effect of which can significantly influence the stress evolution in coal. Mechanical experiments such as uniaxial and triaxial compressive tests have been used to investigate the strain rate dependency of coal mechanical properties, especially Young's modulus and uniaxial compressive strength (UCS) (Fan et al. 2020; Xiao et al. 2020; Khan et al. 2022; Zhong et al. 2021). For instance, Fan et al. (2020) used a split Hopkinson pressure bar (SHPB) to conduct uniaxial compression tests on coal to study its dynamic mechanical response under different loading strain rates. Their results showed that UCS and Young's modulus have apparent strain rate dependency (the faster the loading strain rate, the higher the UCS and Young's modulus of coal specimens). These observations are consistent with results from Xiao et al. (2020), who performed uniaxial compression tests to study the influence of strain rate on coal mechanical properties and failure process. In their study, Young's modulus showed a strong strain rate dependency, especially at high strain rates. Recently, Li et al. (2022) carried out triaxial compression tests on coal specimens to study their mechanical properties and deformation under different strain rates and confining stresses. Their results indicated that the stress–strain response and peak strength of coal samples have a clear strain rate dependency. Also, it was observed that an increase in confining stress intensifies the strain rate dependency of peak strength, but it has no consistent influence on the stress–strain response. It is noted that the above-discussed rate dependency experiments were conducted on dry coal specimens.

Despite the research conducted to date on the viscous behaviour of dry coal specimens, the effect of gas pressure on the coal viscoelastic response has received little attention. The presence of gas is ubiquitous in coal and has an important influence on many engineering problems, such as well completion, wellbore stability, and hydraulic fracturing amongst others (Detournay and Atkinson 2000; Helmons et al. 2016). The rock pore pressure variation during loading can affect the pore and fracture system, and in turn affect the strain rate dependency (Al-Bazali et al. 2008; Zhong et al. 2022). The effect of pore pressure on strain rate-dependent behaviour of rocks is in general, however, complex because of the interactions between boundary conditions of the loading process and the hydromechanical response as observed in some fractured shale rocks (Helmons et al. 2016; Swan et al. 1989). The authors were able to find only a few studies in the literature investigating the effect of pore pressure on strain rate dependency of rock samples where the micro-scale physical processes causing macro-scale experimental observations were not studied. Swan et al. (1989) conducted triaxial compression tests on shale specimens with water to investigate their strain rate-dependent behaviour with water pore pressure. Under undrained condition, almost no strain rate dependency on the mechanical properties of shale was observed, especially for strain rates below 0.1 min^{-1}. This behaviour was linked to pore pressure build-up in the specimen due to undrained testing conditions stiffening the specimens and reducing the viscous effect. In drained testing conditions, their results also showed no rate dependency. It was postulated that water does not have enough time to drain during deviatoric loading due to the low permeability of shale and is trapped in the pores causing localised pore pressure build-up (localised undrained response) which leads to the insensitivity of specimen to different strain rates. For the strain rates above 0.1 min^{-1}, the shale strength, however, increased with the strain rate. A similar observation was made by Brace and Martin (1968), who conducted triaxial compression tests on crystalline silicate rocks with low porosity at different strain rates and pore pressures. Their results showed that specimens have trivial rate dependency for the strain rates lower than a critical value; once the strain rate surpasses this critical value, the rock becomes more competent compared to zero pore pressure. Again, the localised pore pressure increase was used as the hypothesis for such strengthening behaviour (Al-Bazali et al. 2008; Brace and Martin 1968). Al-Bazali et al. (2008) conducted triaxial compression tests on shale specimens and developed a theoretical model to study the impact of strain rate on specimens' mechanical behaviour. In their study, axial loading caused pore pressure build-up under drained conditions due to low shale permeability thus reducing rate dependency of mechanical response. Helmons et al. (2016) used the discrete element method to simulate the rock failure process under different strain rates. In their study, both drained and undrained boundary conditions were considered. Their results indicated that the strength of rock has no rate dependency under undrained conditions when the strain rate is lower than a critical value. These numerical results supported the

experimental results of Swan et al. (1989) and Brace and Martin (1968).

The above studies reveal that the rate-dependent behaviour of dry and gas-saturated specimens is relatively different. However, the micro-processes controlling such macro-scale behaviours have not been fully understood nor systematically analysed. This study, therefore, aims to assess the coal rate dependency at dry and inert gas-saturated conditions systematically and shed light on the microscale processes controlling the coal rate dependency especially with gas pore pressure without sorption. To achieve this, we perform a set of triaxial compressive experiments on dry and gas-saturated specimens under different loading strain rates. To exclude the gas adsorption effect, non-sorbing gas (Helium) was used in the experiments. We further design a set of experiments combining X-ray micro-Computed Tomography (XRCT) scanning with hydromechanical testing to investigate the gas trapping in coal specimens under different loading rates leading to localised undrained conditions.

2 Experimental Methodology

2.1 Samples and Equipment

All experiments were conducted on coal specimens from a coal seam in the eastern coast of Australia. Three cylindrical coal specimens (labelled as S1, S2 and S3) were cored from a highly volatile bituminous coal block and cut to a diameter of 28.5 mm and varying lengths of 51 mm, 62.8 mm and 62.8 mm, respectively, to be used for the hydro-mechanical experiments (cores were cut to a length that could maintain the specimen quality for testing). The porosity of specimens S1, S2 and S3 was also measured using Helium (He) gas-porosimeter to be used for the interpretation of the results. A smaller specimen (labelled as S4) with 12.7 mm in diameter and a length of 25 mm was cored from the same block for the XRCT experiment to investigate the local undrained response postulation discussed earlier. The details of specimens and type of experiments are listed in Table 1.

Two triaxial cells were used in this study for hydromechanical and XRCT experiments, respectively. The large triaxial cell (Roshan et al. 2018) was used to test the coal specimens with different strain rates and Helium pore

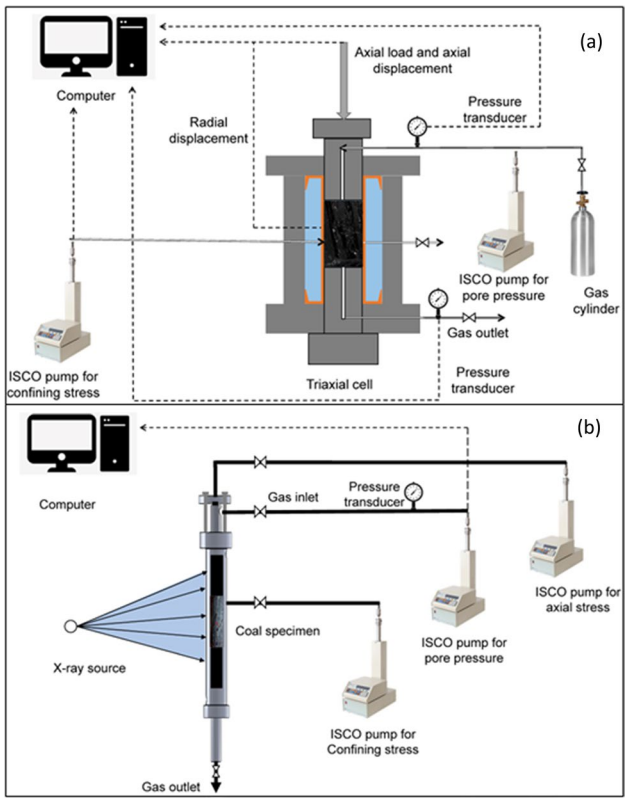

Fig. 1 **a** Experimental setup for coal triaxial experiments under different loading strain rates and pore pressure and **b** experimental setup for XRCT experiments

pressure (Fig. 1a). To perform this set of experiments, a servo-controlled loading frame was used to provide the axial load at a constant displacement rate i.e., constant axial strain rate. The confining stress was provided by a 500D ISCO pump communicating with the loading frame to apply the same axial stress as it increases. This combination ensures that the experiments are run at true constant axial ($\dot{\varepsilon_a}$) and volumetric [$\dot{\varepsilon_v} = (1 + 2\nu)\,\dot{\varepsilon_a}$, where ν is Poisson ratio] strain rates. Another 500D ISCO pump was used to inject the gas into the triaxial cell and pore pressure data were logged by two independent pressure transducers with high accuracy (± 1 psi). Radial displacements were measured by 4 linear variable differential transformers (LVDTs) inside the triaxial cell and recorded using Flexlogger software from National Instruments. A high-resolution (10^{-5} N) load cell with a capacity of 10 kN was used to record the axial load data

Table 1 Details of the specimens and the experimental scenarios

Specimens	Diameter (mm)	Length (mm)	Type of experiment	Gas
S1	28.5	51	Triaxial	Helium
S2	28.5	62.8	Triaxial	Helium
S3	28.5	62.8	Triaxial	Helium
S4	12.7	25	Loading with XRCT imaging	Krypton

very accurately (independent from a recording by servo-controlled loading frame).

To precisely visualize, map and characterize the microstructural changes of specimen S4 (due to gas intake and mechanical loading with different loading rates), a small X-ray transparent triaxial cell was used for XRCT experiments (Roshan et al 2019) (Fig. 1b). The axial and confining stresses were applied by 500D ISCO pumps with hydraulic oil. Another 500D ISCO pump was used to provide pore pressure and monitor the amount of intake/expelled gas volume. The Krypton gas was used in the XRCT experiments because of its high attenuation coefficient (Mccrary 1971). The amount of injected gas was logged using ISCO pump software and pore pressure was monitored by pressure transducers. For XRCT imaging, a high-resolution helical micro-CT scanner was used; the detail of which can be found in (Pirzada et al. 2018). The obtained grayscale images from XRCT measurements were analysed using Avizo software; the image processing is discussed in the next section. All experiments were conducted at room temperature.

2.2 Experimental Procedure

2.2.1 Triaxial Experiments on Coal Specimens Under Different Loading Strain Rates

Two sets of experiments were designed and performed on coal specimens to characterize their strain rate-dependent mechanical behaviour and investigate the effect of pore pressure on their rate-dependent behaviour. The first set of triaxial experiments was conducted on specimens S1, S2 and S3 at both dry and Helium saturated condition (with different pore pressures of 0.5, 1 and 1.5 MPa) and axial displacement rates ranging from 0.12 to 0.6 mm/min (leading to axial strain rates of 3×10^{-5} s^{-1} to 2×10^{-4} s^{-1}). In this paper, the dry condition refers to specimens that are not saturated with Helium and Krypton and filled with air at atmospheric pressure. These experiments were conducted under drained conditions where a pump controlled the internal pore pressure. In addition, the isotropic external loading was set up leading to constant axial and volumetric strain rates as stated previously. For experiments conducted on dry specimens, the effective isotropic stress of up to 3 MPa was applied. The relatively low-stress value was used to ensure that only elastic deformation is experienced by the specimens and any damage is avoided (the specific coal specimen's UCS is ~ 7–8 MPa). It is noted that each loading was followed by an unloading stage where the displacement was recorded to ensure no permanent deformation (damage) occurs.

To perform the experiment, the first axial strain rate is applied until reaching 3 MPa while confining pressure tracks the axial stress thus an isotropic state of stress is maintained. The stress is then released until the specimen comes back to zero strain, and the next strain rate is then applied. As abovementioned, this procedure allows us to monitor any permanent deformation (damage) in the specimen by tracking the recovered strain. The rate-dependent bulk modulus can be also calculated using Eq. (1) (Detournay and Cheng 1993), where P_c is the isotropic (hydrostatic) stress and ε_v is volumetric strain.

$$K = \frac{\Delta P_c}{\Delta \varepsilon_v} \tag{1}$$

For experiments with pore pressure, Helium was injected into specimens with pressures of 0.5, 1 and 1.5 MPa; the maximum isotropic stress and axial strain rates were the same as experiments performed on dry specimens.

To perform the experiments with pore pressure, 1 MPa initial isotropic stress was set and then Helium was injected into the specimen at 0.5 MPa pore pressure. The initial isotropic stress was set to be slightly higher than pore pressure to avoid gas leakage. Two pressure transducers on the upstream and downstream side of the triaxial cell were used to ensure that the specimen was fully saturated by Helium. Once the pressure was stable, the isotropic stress was increased at a constant strain rate to 3 MPa while pore pressure was kept constant at 0.5 MPa using a back pressure regulator. After the first loading rate was tested, the stress

Table 2 Testing conditions for specimens S1, S2 and S3 with different pore pressures and loading strain rates

Specimen	Isotropic stress (MPa)	Pore pressure (MPa)	Loading strain rate (s^{-1})
S1	Up to 3	0, 0.5, 1, 1.5	4×10^{-5}
			6×10^{-5}
			1×10^{-4}
			1.4×10^{-4}
			2×10^{-4}
S2	Up to 3	0, 0.5, 1, 1.5	3×10^{-5}
			5×10^{-5}
			8×10^{-5}
			1×10^{-4}
			1.6×10^{-4}
S3	Up to 3	0, 0.5, 1, 1.5	3×10^{-5}
			5×10^{-5}
			8×10^{-5}
			1×10^{-4}
			1.6×10^{-4}
S4	Up to 5	1	Fast loading (0 to 5 MPa in 5 s)
			Slow loading (0 to 5 MPa in 30 min)

was released until the specimen comes back to zero strain and the next strain rate was applied. Once the first pore pressure for all strain rates was completed, the pore pressure was increased to the next pressure (1 MPa) and initial isotropic stress was increased to 1.5 MPa and the same procedure for each strain rate was repeated. Finally, a pore pressure of 1.5 MPa with initial isotropic stress of 2 MPa was set, and different strain rates were used for stress measurements. The abovementioned experimental steps were repeated for specimens S2 and S3. The details of the testing conditions on specimens S1, S2 and S3 can be seen in Table 2.

2.2.2 Measuring Effective Stress Coefficients of Coal Specimens

To enable comparing the results between different pore pressures, the experiments should be analysed and compared at the same effective stress level. The conventional approach is to simply use "effective stress (σ') = total stress (σ_t)—pore pressure (p)" ignoring the skeleton effect. If the skeleton effect is to be considered, then the effective stress coefficient, ESC (i.e., Biot coefficient for porous rocks, α) should be characterised ($\sigma' = \sigma_t - \alpha p$). It is noted that the study by Lv et al. (2021) showed the Biot coefficient is applicable in cleated coals despite that coal is not a pure porous medium. To measure the ESC (α), the bulk (K) and solid bulk modulus (K_s) are required (Franquet and Abass 1999):

$$\alpha = 1 - \frac{K}{K_s} \tag{2}$$

To measure the solid bulk modulus, a step undrained triaxial experiment is carried out (Salemi et al. 2021) where K_s is calculated (Detournay and Cheng 1993):

$$K_s = \left.\frac{\Delta P_c}{\Delta \varepsilon_v}\right|_{P_c = p} \tag{3}$$

where p is the pore pressure and ΔP_c and $\Delta \varepsilon_v$ are a step change in isotropic stress and resultant volumetric strain, respectively. In the measurement of K_s, 1 MPa initial isotropic stress was applied followed by 0.5 MPa Helium pressure injection where the volumetric strain was recorded. The isotropic stress was then increased to 1.5 MPa followed by an increase in pore pressure to 1 MPa. Finally, the isotropic stress was increased to 2 and 2.5 MPa followed by an increase in pore pressure to 1.5 and 2 MPa, respectively. The plot of isotropic stress versus volumetric strain returns the solid bulk modulus. The bulk modulus is the slope of isotropic stress to the volumetric strain line already performed as part of rate-dependent experiments in Sect. 2.2.1.

2.2.3 XRCT Experiments on Coal with Pore Pressure

The XRCT technique has been widely used to observe the material's internal structure and failure mechanisms in three dimensions (Karacan 2007; Lv et al. 2022; Özgen Karacan 2003; Pirzada et al. 2018; Pone et al. 2010; Sukop et al. 2008). The fracture-matrix interaction of coal with stress and pore pressure can significantly affect the gas distribution. As discussed earlier, the pore pressure is believed to reduce the viscous rate dependency of porous geomaterials but no experimental evidence for such a claim especially at the micro-scale exists. To shed light on the effect of pore pressure on rate dependency in coal, another set of novel experiments was conducted on a smaller coal specimen, S4 involving XRCT imaging using highly visible noble gas (Krypton). The experiment involved saturating the coal specimen, S4 with Krypton at a pore pressure of 1 MPa. The loading stress and pore pressure on the specimen were kept constant for 68 h to fully saturate the specimen before it was scanned at its initial condition. The loading was then applied at a slow and a fast rate (5 MPa isotropic stress applied in 5 s and 30 min, respectively) while the drained condition is maintained by an ISCO pump and back pressure regulator. The specimen was scanned (XRCT) at each stage. Initially, the slow loading was applied to reach 5 MPa pressure in 30 min (starting from the initial 1.5 MPa isotropic stress applied to enable injecting 1 MPa gas). The stress was then removed, and time was given so that the gas distribution goes back to its initial condition before the fast rate is applied. The pumped gas volume was recorded continuously. The obtained image resolution was ~ 18.2 µm. The Avizo software was used for image processing including gray-scale intensity equilibration, registration, and subtraction.

The image processing involved gray-scale equilibration initially. The grayscale intensity might be slightly different

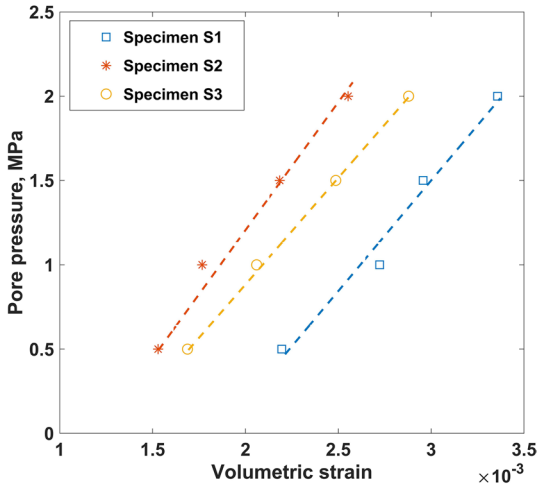

Fig. 2 Obtaining solid bulk modulus of specimens S1, S2 and S3

from one measurement to another due to variations in X-ray instrument measurement. We thus selected specific points (rubber, cell body, hydraulic oil) between different images and equilibrated the gray-scale intensities between them. This procedure ensures that later subtraction of the images results in actual differences and not propagated noises. Next, the images were registered by bringing them into geometric alignment using a 3D image registration technique developed by (Latham et al. 2008). This enables voxel-to-voxel comparisons between the images obtained before and after the experiments. Once equilibration and registration were completed, the images (their gray-scale intensities) were subtracted from each other to visualise the difference between the images. The change in gas intensity between different experiments can prove local gas pressure build-up that can lead to fading viscous rate dependency of the specimens. It is noted that no image segmentation is required in the analysis as the gray-scale intensity change is representative of the gas concentration difference between images because nothing else in the specimen changes between the two scans.

3 Experimental Results

In order to analyse the viscoelastic response of the specimens, the effective stress values should be obtained ($\sigma' = \sigma_t - \alpha p$); the values of which are required for calculating the effective stress coefficient (Biot 1941). Figure 2 shows the results of the solid bulk modulus (K_s) of specimens S1, S2 and S3 (Adelina et al. 2019). Having the solid bulk modulus and bulk modulus, the effective stress coefficient can be calculated using Eq. 2 which in turn enables calculating the effective stress values. It is noted that the bulk modulus of each strain rate and solid bulk modulus of each specimen were used to calculate the effective stress coefficient of the specimen at every test.

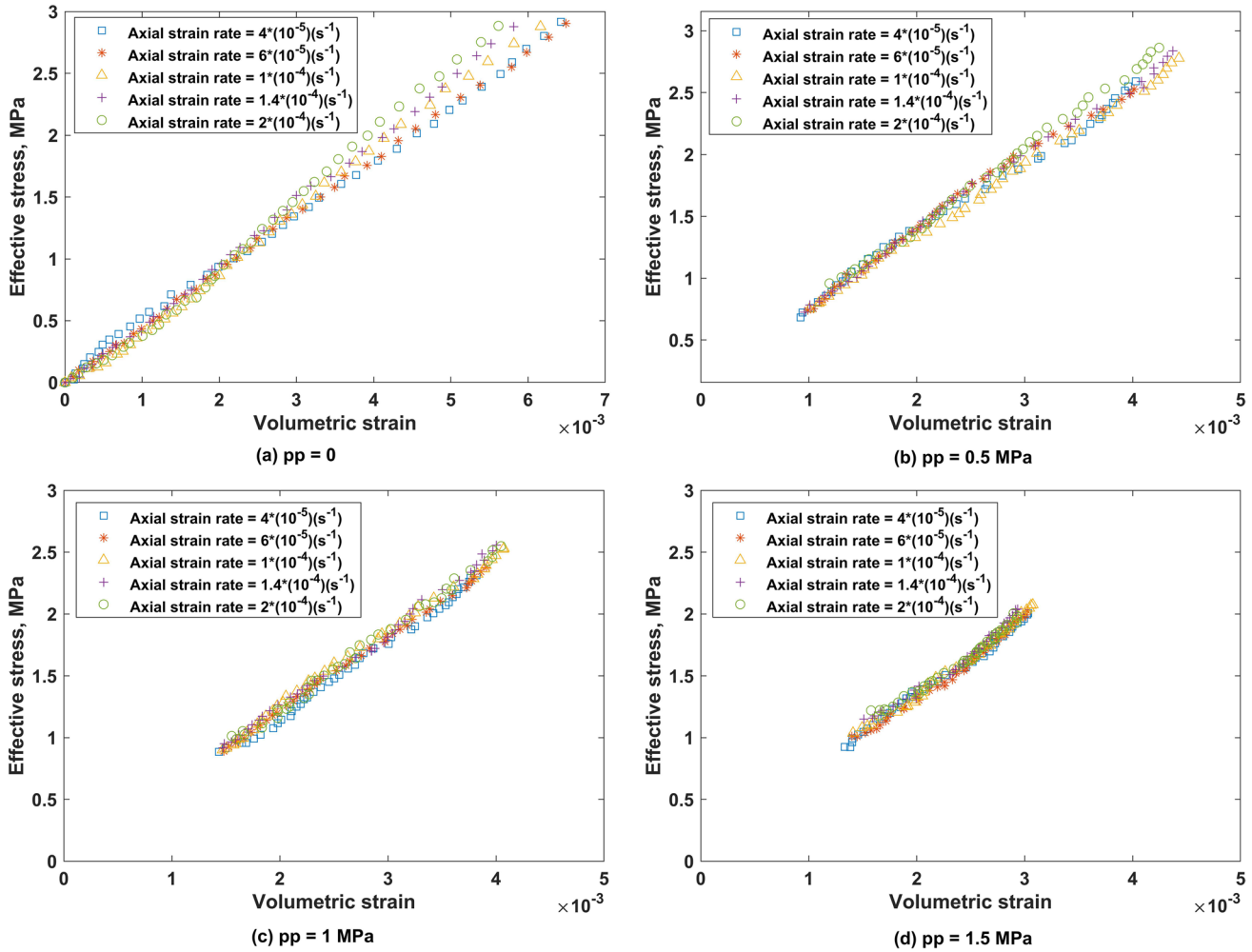

Fig. 3 The effective stress versus volumetric strain for the specimen, S1 under different pore pressures and strain rates: **a** dry condition, **b** pore pressure of 0.5 MPa, **c** pore pressure of 1 MPa, and (**d** pore pressure of 1.5 MPa

The results of rate-dependent experiments on specimen S1 under dry and different pore pressures (0.5, 1, 1.5 MPa) are shown in Fig. 3. Figure 3(a) shows the evolution of effective isotropic stress (at zero pore pressure) versus volumetric strain for different strain rates. It is seen from this figure that stress–strain relations are identical for low strain rates of 4×10^{-5} and 6×10^{-5} s^{-1} meaning a negligible strain rate dependency under these strain rates. The slope of effective isotropic stress versus volumetric strain curve represents the bulk modulus of the specimen under different loading strain rates. When the strain rate reaches a threshold (approximately 6×10^{-5} s^{-1}) for this specimen (S1), the stress–strain relation starts to show clear rate-dependent behaviour leading to bulk modulus increase with an increase in strain rates. These experimental results on coal specimens under dry conditions are consistent with previous studies (Fan et al. 2020; Xiao et al. 2020).

Figure 3(b–d) further present results of effective isotropic stress versus volumetric strain of specimen S1 at different strain rates for pore pressure of 0.5, 1.0 and 1.5 MPa, respectively. The effect of pore pressure on strain rate-dependent behaviour can be seen by comparing Fig. 3(a–d). The results evidently show that under the same effective stress, the strain rate dependency decreases significantly with the introduction of pore pressure. The specimen under a higher strain rate of 2×10^{-4} s^{-1} still shows some level of rate dependency at 0.5 MPa pressure but such rate dependency vanishes toward higher pore pressures e.g., no strain rate dependency is observed at 1.5 MPa pore pressure. These results confirm that an increase in pore pressure reduces the strain rate dependency of coal specimen, S1.

Figures 4 and 5 show the results of strain rate-dependent experiments on coal specimens, S2 and S3, respectively. For dry conditions, both specimens show similar rate-dependent stress–strain relations where a higher strain rate increases the

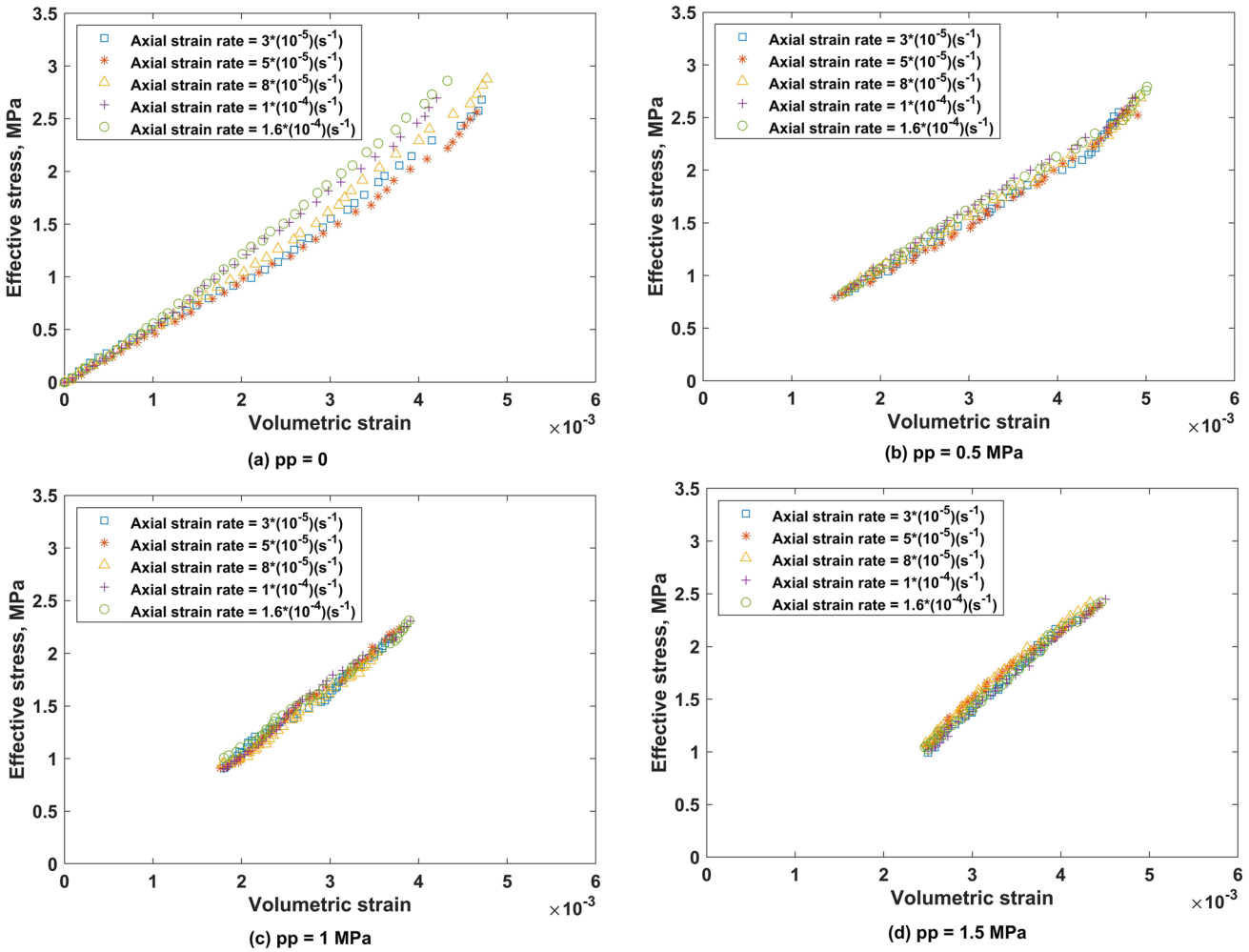

Fig. 4 The effective stress versus volumetric strain for the specimen, S2 under different pore pressures and strain rates: **a** dry condition, **b** pore pressure of 0.5 MPa, **c** pore pressure of 1 MPa, and **d** pore pressure of 1.5 MPa

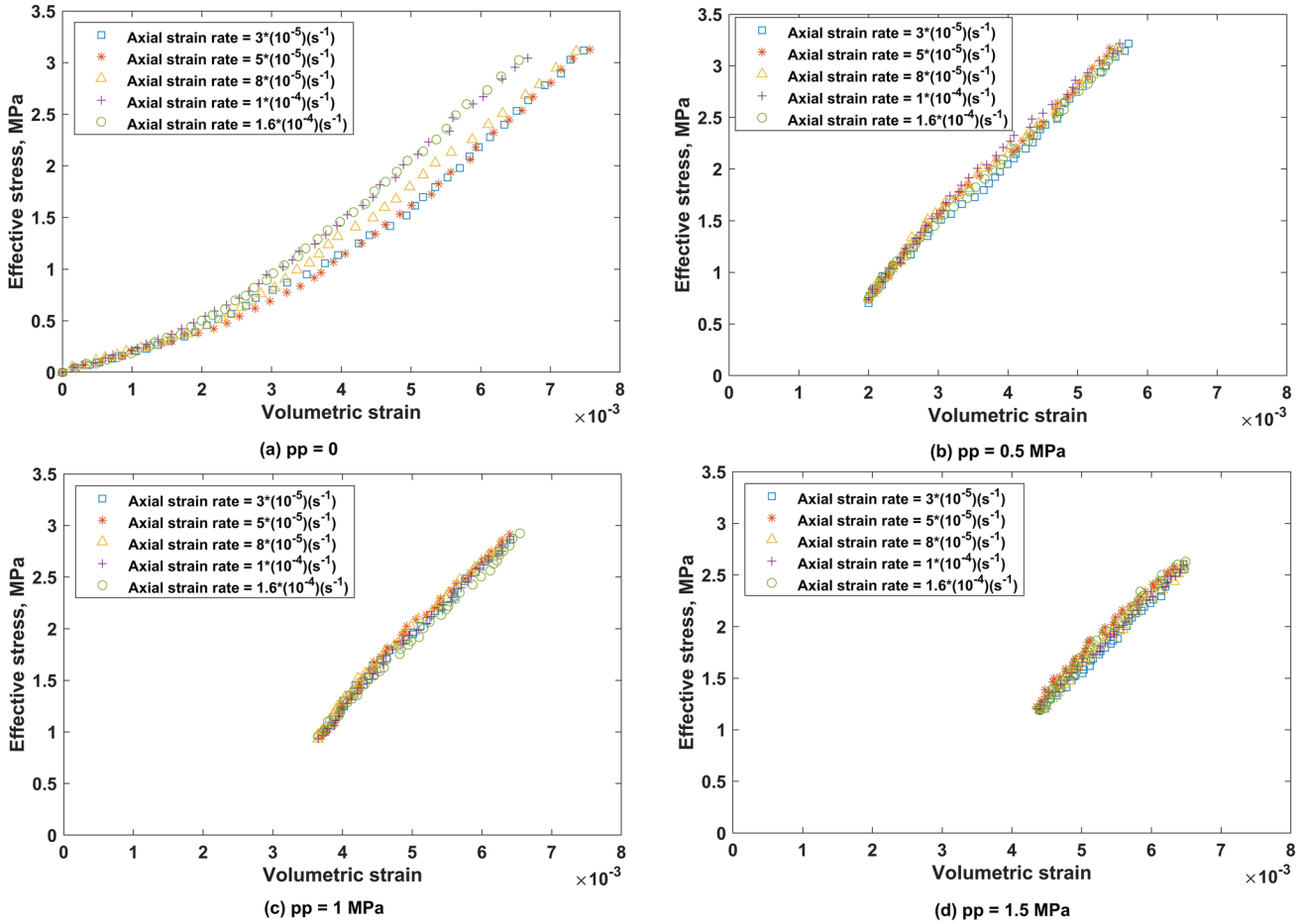

Fig. 5 The effective stress versus volumetric strain for the specimen, S3 under different pore pressures and strain rates: **a** dry condition, **b** pore pressure of 0.5 MPa, **c** pore pressure of 1 MPa, and **d** pore pressure of 1.5 MPa

Fig. 6 X-ray tomography of specimen, S4 saturated with Krypton (Lighter gray represents the higher concentration of Krypton)

rate dependency and the bulk modulus of coal specimens. Similar to specimen S1, specimen S3 shows a clear rate-dependency at strain rates above approximately $5 \times 10^{-5} s^{-1}$. The specimen S2 shows rate-dependency at all axial strain rates under dry conditions. The rate-dependent behaviour of specimens S2 and S3, similar to specimen S1, reduces significantly with an increase in pore pressure. At a pore pressure of 1.0 MPa, no rate dependency is observed for specimens S2 nor S3.

The strain rate-dependent testing of specimens S1, S2 and S3 individually and collectively show that pore pressure at drained condition reduces the rate dependency. Specialized experimental design is required to investigate the physical mechanisms responsible for such behaviour, especially at micro-scale. We thus designed a set of XRCT experiments on specimen, S4 as previously explained. Figure 6 shows a grayscale 3D tomograph of specimen S4 at the initial condition with Krypton gas pressure of 1 MPa and isotropic stress of 1.5 MPa. The lighter gray represents the areas with a higher concentration of Krypton. In the XRCT experiments,

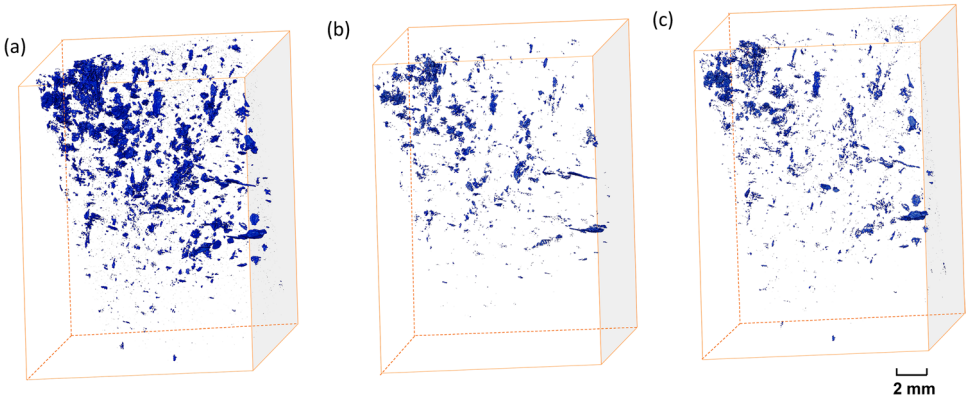

Fig. 7 XRCT results of the experiments on coal specimen, S4 under different loading rates with 1 MPa Krypton gas pressure and 1.5 MPa isotropic stress **a**: the difference in grayscale intensity of the specimen between images captured at faster loading test and initial condition. **b**: the difference in grayscale intensity of the specimen between images captured at slower loading test and initial condition and **c**: the difference in grayscale intensity of the specimen between images captured at faster and slower loading tests

the specimen, S4 was fully saturated with Krypton gas at the initial condition and then loading was applied at two different loading speeds (fast and slow) as previously explained.

Figure 7 shows the XRCT results of the experiments on coal specimen (S4) under different loading rates with 1 MPa Krypton gas pressure and 1.5 MPa isotropic stress where (a) represents the difference of grayscale intensity of specimen between images captured at faster loading test and initial condition, (b) the difference of grayscale intensity of specimen between images captured at slower loading test and initial condition and (c) the difference of grayscale intensity of specimen between images captured at faster and slower loading tests. The XRCT images from each two condition were registered to ensure the images can be compared before subtracting the grayscale intensity.

Figure 7 interestingly shows that although the drained condition was maintained throughout the fast and slow tests (isotropic loading), some gas was trapped inside the specimen and caused an increase in grayscale intensity (representing higher gas concentration). From this figure, it is seen that the gas trapped in the specimen has localised higher pressures (higher intensity thus concentration and pressure) when the load is applied to the specimen. Such gas trapping is considerably higher when the loading rate is fast [Fig. 7(a)]. It is intuitive that higher loading rates will close micro-fractures and pores and compress the trapped gas with an increase in volumetric strain. This compression of the trapped gas leads to an increase in pore pressure locally causing localised undrained response. Such an undrained response strengthens the specimen thus reducing the rate-dependent behaviour. Previous studies on sedimentary rocks indicated similar behaviour. For example, Swan et al. (1989) conducted triaxial tests on shale specimens under both drained and undrained conditions. They hypothesized that pore pressure inside the specimen can be higher than the measured pore pressure values during compression even under drained conditions leading to reduced rate-dependency of shale specimens which is supported by our observations.

4 Discussion

Our experimental results show apparent rate-dependency of dry coal specimens where the higher strain rates increase the specimen bulk modulus. Previous studies postulated different mechanisms for such rate dependency. One mechanism of strain rate-dependent mechanical properties of rock, for example, is related to the compaction-induced pre-existing micro-fractures closure during the isotropic loading process (Helmons et al. 2016; Liang et al. 2011). The faster the isotropic loading, the faster the pre-existing micro-factures closure causing a strengthening effect on the specimen and increasing its bulk modulus. Another proposed mechanism for such a hardening effect induced by high strain rates is linked to fracture development changing from macroscopic fracturing at low strain rates to micro-cracking at high strain rates (Hou et al. 2019). It is noted that the proposed mechanisms of rate dependency are often related to fracture development in specimens under different loading rates. In this study, 3 MPa effective isotropic (hydrostatic) stress was applied in all tests which are relatively low compared to UCS of specimens (7–8 MPa). In addition, the unloading was followed by each loading stage to monitor any permanent deformation (damage) and ensure only an elastic deformation (no damage) is experienced. This in turn rolls out the effect of micro-fracture generation on strain-rate dependency. Therefore, only the pre-existing fractures are likely to affect the strain-rate dependency.

It can be seen from the experimental results (Figs. 3, 4 and 5) that specimens S1 and S3 show relatively similar

rate-dependent behaviour which is different from specimen S2. When looking at the stress–strain results of these specimens, it is observed that specimens S1 and S3 reach around 6.5×10^{-3} volumetric strain value at 3 MPa effective stress while specimen S2 experiences only 4.5×10^{-3} volumetric strain value at 3 MPa effective stress magnitude. Knowing that (i) the compressibility of fractures is much higher than matrix, (ii) the matrix compressibility of the three specimens are similar (sister cores) and (iii) the coal specimens are cleated and are under low stresses (< 3 MPa), it can be concluded that the specimens S1 and S3 have similar fracture systems. The porosity measurement of the specimens S1 and S3, however, returned different porosities of 2.57% and 5.46%, respectively, yet these two specimens show similar volumetric strain responses. Considering that the matrix porosity across specimens is similar, the difference in porosity indicates different fracture porosity e.g., specimen S3 has higher fracture porosity than specimen S1. The same volumetric response across two specimens with different fracture porosities, therefore indicates that fracture stiffness should dominate the volumetric strain development. Where the fracture stiffness is a dominant factor controlling the strain, one expects that it should also control the strain evolution with external loading rates.

The results of rate dependency of different coal specimens under dry condition and different pore pressures are evident for this observation (Figs. 3, 4 and 5). This observation cannot be linked to poroelastic response as all experiments were conducted at the same effective stress. Thus, other processes should be involved to observe less rate dependency with higher pore pressure. Al-Bazali et al. (2008) conducted experimental and theoretical studies to investigate the effect of strain rate on the failure characteristics of shale. They postulated that pore pressure build-up can occur in the specimen under drained conditions where the rate of pore pressure build-up depends on the strain rate. Higher the strain rate, the higher the pore pressure build-up both in its rate and eventual magnitude. Other numerical studies on intact (Roshan and Aghighi 2012) and fractured shale (Roshan and Fahad 2012) also showed that localised undrained response can occur in low permeable formations under drained conditions.

Although coal is a fractured sediment and different from shale in terms of permeability, the small-scale cleats/fractures can act as gas-trapping sites under different loading rates. We proved this postulation using our XRCT experiments (Fig. 7) where gas can be trapped inside the specimen during isotropic loading, especially at a faster loading rate. The trapped gas and its associated pressure increment leads to localised undrained response under drained testing conditions. This in turn causes the specimen to strengthen thus reducing the rate dependency. We, therefore, conclude that the interaction of gas and macropores–microfractures is the process controlling the rate dependency in coal samples.

5 Conclusion

This study investigates the effect of non-sorptive gas pore pressure on strain rate-dependent mechanical behaviour of coal specimens systematically. A series of triaxial experiments with different strain rates were conducted on both dry specimens and specimens saturated with pressured Helium. Another set of experiments combined with the X-ray micro-CT (XRCT) scanning technique was conducted to obtain the gas distribution in the specimen under different loading rates and to assist in understanding the effect of pore pressure on the strain rate-dependent behaviour of the specimens. The experimental results show clear rate-dependent stress and strain relation of coal specimens under dry conditions where the rate-dependency increases with strain rates. The higher strain rates cause an apparent stiffening effect on specimens and increase their bulk modulus. This rate-dependency, however, decreases significantly with the increase of pore pressure. The results of XRCT experiments demonstrate that gas can be trapped inside the coal specimen during isotropic loading, especially at a higher loading speed. This in turn leads to a localised undrained response in an apparently drained experiment causing the specimen strengthening effect and reducing the rate-dependency of coal. The coupled effect of sorption on the viscoelastic response of coal is more complicated and is a focus of our future investigations.

Author Contribution LS: Writing original draft, Conceptualization, Methodology, Investigation, Visualization. MAQS: Methodology, Investigation, reviewing and editing. HR: Conceptualization, Methodology, funding acquisition, supervision, writing—reviewing and editing.

Funding Open Access funding enabled and organized by CAUL and its Member Institutions.

Data availability The data that support the findings of this study are available from the corresponding author upon request.

Declarations

Conflict of Interest The authors declare that they have no known competing financial interests that could have appeared to influence the work reported in this paper.

References

Adelina L, Hossein M, Hamid R (2019) Biot coefficient of gas sorbing rocks: a coal example, 53rd U.S. Rock Mechanics/Geomechanics Symposium

Aghighi MA, Lv A, Roshan H (2021) Non-equilibrium thermodynamics approach to mass transport in sorptive dual continuum porous media: a theoretical foundation and numerical simulation. J Nat Gas Sci Eng 87:103757. https://doi.org/10.1016/j.jngse.2020.103757

Aghighi MA, Lv A, Siddiqui MAQ, Masoumi H, Thomas R, Roshan H (2022) A multiphysics field-scale investigation of gas pre-drainage in sorptive sediments. Int J Coal Geol 261:104098. https://doi.org/10.1016/j.coal.2022.104098

Al-Bazali T, Zhang J, Chenevert ME, Sharma MM (2008) Experimental and numerical study on the impact of strain rate on failure characteristics of shales. J Petroleum Sci Eng 60:194–204. https://doi.org/10.1016/j.petrol.2007.09.001

Biot MA (1941) General theory of three-dimensional consolidation. J Appl Phys 12:155–164. https://doi.org/10.1063/1.1712886

Brace WF, Martin RJ (1968) A test of the law of effective stress for crystalline rocks of low porosity. Int J Rock Mech Min Sci Geomech Abstr 5:415–426. https://doi.org/10.1016/0148-9062(68)90045-4

Cao A, Jing G, Ding Y-L, Liu S (2019) Mining-induced static and dynamic loading rate effect on rock damage and acoustic emission characteristic under uniaxial compression. Saf Sci 116:86–96. https://doi.org/10.1016/j.ssci.2019.03.003

Detournay E, Atkinson C (2000) Influence of pore pressure on the drilling response in low-permeability shear-dilatant rocks. Int J Rock Mech Min Sci 37:1091–1101. https://doi.org/10.1016/S1365-1609(00)00050-2

Detournay E, Cheng AHD (1993) 5—fundamentals of poroelasticity. In: Fairhurst C (ed) Analysis and design methods. Pergamon, Oxford, pp 113–171

Espinoza DN, Vandamme M, Dangla P, Pereira JM, Vidal-Gilbert S (2016) Adsorptive-mechanical properties of reconstituted granular coal: experimental characterization and poromechanical modeling. Int J Coal Geol 162:158–168. https://doi.org/10.1016/j.coal.2016.06.003

Fan C, Li S, Elsworth D, Han J, Yang Z (2020) Experimental investigation on dynamic strength and energy dissipation characteristics of gas outburst-prone coal. Energy Sci Eng 8:1015–1028. https://doi.org/10.1002/ese3.565

Franquet JA, Abass HH (1999) Experimental evaluation of Biot's poroelastic parameterThree different methods, Vail Rocks 1999, The 37th U.S. Symposium on Rock Mechanics (USRMS)

Helmons RLJ, Miedema SA, Rhee Cv (2016) Simulating hydro mechanical effects in rock deformation by combination of the discrete element method and the smoothed particle method. Int J Rock Mech Min Sci 86:224–234. https://doi.org/10.1016/j.ijrmms.2016.04.018

Hou Z, Gutierrez M, Ma S, Almrabat A, Yang C (2019) Mechanical behavior of shale at different strain rates. Rock Mech Rock Eng 52:3531–3544. https://doi.org/10.1007/s00603-019-01807-7

Karacan CÖ (2007) Swelling-induced volumetric strains internal to a stressed coal associated with CO2 sorption. Int J Coal Geol 72:209–220. https://doi.org/10.1016/j.coal.2007.01.003

Khan NM, Ma L, Cao K, Spearing AJS, Liu W, Jie Y, Yousaf M (2022) Early violent failure precursor prediction based on infrared radiation characteristics for coal specimens under different loading rates. Rock Mech Rock Eng 55:6939–6961. https://doi.org/10.1007/s00603-022-03021-4

Latham S, Varslot T, Sheppard A (2008) Image registration: enhancing and calibrating X-ray micro-CT imaging. Proc. Of the Soc. Core Analysts, Abu Dhabi, UAE, 1–12

Li Y, Yang S-Q, Liu Z-L, Sun B-W, Yang J, Xu J (2022) Study on mechanical properties and deformation of coal specimens under different confining pressure and strain rate. Theor Appl Fract Mech 118:103287. https://doi.org/10.1016/j.tafmec.2022.103287

Liang WG, Zhao YS, Xu SG, Dusseault MB (2011) Effect of strain rate on the mechanical properties of salt rock. Int J Rock Mech Min Sci 48:161–167. https://doi.org/10.1016/j.ijrmms.2010.06.012

Lv A, Aghighi MA, Masoumi H, Roshan H (2021) The effective stress coefficient of coal: a theoretical and experimental investigation. Rock Mech Rock Eng 54:3891–3907. https://doi.org/10.1007/s00603-021-02476-1

Lv A, Bahaaddini M, Masoumi H, Roshan H (2022) The combined effect of fractures and mineral content on coal hydromechanical response. Bull Eng Geol Env 81:172. https://doi.org/10.1007/s10064-022-02669-0

Mccrary J (1971) Attenuation coefficients of gases for 4.5 TO 145 keV photons. J Phys Colloques. https://doi.org/10.1051/jphyscol:1971404

ÖzgenKaracan C (2003) An effective method for resolving spatial distribution of adsorption kinetics in heterogeneous porous media: application for carbon dioxide sequestration in coal. Chem Eng Sci 58:4681–4693. https://doi.org/10.1016/j.ces.2003.05.002

Perera MSA, Sampath KHSM (2020) Modelling of free and adsorbed CO2-induced mechanical property alterations in coal. Int J Coal Geol 217:103348. https://doi.org/10.1016/j.coal.2019.103348

Pirzada MA, Zoorabadi M, LameiRamandi H, Canbulat I, Roshan H (2018) CO2 sorption induced damage in coals in unconfined and confined stress states: a micrometer to core scale investigation. Int J Coal Geol 198:167–176. https://doi.org/10.1016/j.coal.2018.09.009

Pone JDN, Halleck PM, Mathews JP (2010) 3D characterization of coal strains induced by compression, carbon dioxide sorption, and desorption at in-situ stress conditions. Int J Coal Geol 82:262–268. https://doi.org/10.1016/j.coal.2009.11.010

Roshan H, Aghighi MA (2012) Analysis of pore pressure distribution in shale formations under hydraulic, chemical, thermal and electrical interactions. Transp Porous Media 92:61–81. https://doi.org/10.1007/s11242-011-9891-x

Roshan H, Fahad M (2012) Chemo-poroplastic analysis of a borehole drilled in a naturally fractured chemically active formation. Int J Rock Mech Min Sci 52:82–91. https://doi.org/10.1016/j.ijrmms.2012.03.004

Roshan H, Lv A, Xu YB, Masoumi H, RegenauerLieb K (2018) New generation of hoek cells. Geotech Test J. https://doi.org/10.1520/GTJ20170110

Roshan H, Chen X, Pirzada MA, Regenauer-Lieb K (2019) Permeability measurements during triaxial and direct shear loading using a novel X-ray transparent apparatus: fractured shale examples from Beetaloo basin, Australia. NDT&E Int 107. https://doi.org/10.1016/j.ndteint.2019.102129

Salemi H, Yurikov A, Lebedev M, Behnoudfar P, Rezagholilou A, Iglauer S, Roshan H, Sarmadivaleh M (2021) A novel approach to determine the Biot's coefficient using X-ray computed tomography. Bull Eng Geol Env 80:7865–7877. https://doi.org/10.1007/s10064-021-02405-0

Song H, Zhao Y, Wang J, Jiang Y, Wang X (2021) Loading rates dependency of strength anisotropy in coal: based on the three-dimensional reconstruction modeling technology. Energy Sci Eng 9:855–864. https://doi.org/10.1002/ese3.862

Sukop MC, Huang H, Lin CL, Deo MD, Oh K, Miller JD (2008) Distribution of multiphase fluids in porous media: comparison between lattice Boltzmann modeling and micro-x-ray tomography. Phys Rev E. https://doi.org/10.1103/PhysRevE.77.026710

Swan G, Cook J, Bruce S, Meehan R (1989) Strain rate effects in Kimmeridge bay shale. Int J Rock Mech Min Sci Geomech Abstr 26:135–149. https://doi.org/10.1016/0148-9062(89)90002-8

Van Eeckhout EM (1976) The mechanisms of strength reduction due to moisture in coal mine shales. Int J Rock Mech Min Sci Geomech Abstr 13:61–67. https://doi.org/10.1016/0148-9062(76)90705-1

Xiao W, Zhang D, Cai Y, Chu Y (2020) Study on loading rate dependence of the coal failure process based on uniaxial compression test. Pure Appl Geophys 177:4925–4941. https://doi.org/10.1007/s00024-020-02513-0

Zhao Y, Liu S, Jiang Y, Wang K, Huang Y (2016) Dynamic tensile strength of coal under dry and saturated conditions. Rock Mech Rock Eng 49:1709–1720. https://doi.org/10.1007/s00603-015-0849-0

Zhong K, Zhao W, Qin C, Chen W (2021) Experimental study on the mechanical behavior and failure characteristics of layered coal at medium strain rates. Energies. https://doi.org/10.3390/en14206616

Zhong C, Zhang Z, Ranjith PG, Zhang C, Xue K (2022) The role of pore pressure on the mechanical behavior of coal under undrained cyclic triaxial loading. Rock Mech Rock Eng 55:1375–1392. https://doi.org/10.1007/s00603-021-02705-7